



## Multifunctional membranes for lipidic nanovesicle capture

Simona Salerno<sup>a</sup>, Sabrina Morelli<sup>a</sup>, Antonella Piscioneri<sup>a</sup>, Mariangela Frangipane<sup>a</sup>,  
Alessandro Mussida<sup>b</sup>, Laura Sola<sup>b</sup>, Roberto Frigerio<sup>b</sup>, Alessandro Strada<sup>b</sup>, Greta Bergamaschi<sup>b</sup>,  
Alessandro Gori<sup>b</sup>, Marina Cretich<sup>b</sup>, Marcella Chiari<sup>b</sup>, Loredana De Bartolo<sup>a,\*</sup>

<sup>a</sup> Institute on Membrane Technology, National Research Council of Italy, ITM-CNR, via P. Bucci, cubo 17/C, I-87036 Rende (CS), Italy

<sup>b</sup> Institute of Chemical Sciences and Technologies "G. Natta", National Research Council of Italy, SCITEC-CNR, Via Mario Bianco 9, 20131 Milan, Italy

### ARTICLE INFO

#### Keywords:

Membrane  
Copolymer coating  
Peptide conjugation  
Filtration  
Nanovesicles capture

### ABSTRACT

Tangential flow filtration membrane systems are employed for the isolation and concentration of extracellular vesicles. However, interfacial interactions between the membrane surface and species influence the flux and membrane performance. Here we propose a strategy aimed at introducing functional ligands over the membrane surface to improve the separation process through combined size-exclusion and affinity-based mechanisms, avoiding the binding of contaminants and other non-target molecules. Polysulfone membranes were modified by a nanometric coating of differently functionalized copolymers with the dual purpose of limiting non-specific interactions while promoting the chemoselective conjugation of a membrane-sensing peptide ligand (BPT) for lipid nanovesicles capture. Copoly azide polymer coating positively affects the physico-chemical properties of the membrane, improving filtration performance and antifouling capacity. A decrease of the flux decline ratio from  $38.7 \pm 3.9\%$  to  $21.2 \pm 2.4\%$  and an increase of the ratio of protein permeate concentration ( $C_p$ ) to the respective feed concentration ( $C_f$ ) to values of 0.97 was measured after coating the membrane with c-(DMA-N<sub>3</sub>-BP-MAPS) highlighting its capability to reduce protein adsorption. In addition, the BPT-functionalized membrane displayed a high capturing efficiency towards synthetic liposomes which, notably, can be promptly released upon mild treatment with a divalent cation solution. Overall, our work integrates conventional TFF principles with affinity-based isolation, broadening TFF perspective applications.

### 1. Introduction

Membranes are widely used in bioseparation due to their selective properties and modular nature that allows upscaling and downscaling separation processes. This technology finds important application in the biomedical field and clinical treatment for the replacement of organ functions [1–5]. Membranes have a great potential in the separation, concentration, and purification of subcellular components, with uses such as drug targets, therapeutics, diagnostic biomarkers, and drug-delivery systems. Extracellular vesicles (EVs) play an essential role in intercellular communication transferring cargos from one cell to another [6]. They contain genetic molecules (e.g., DNA, microRNA, mRNA) and proteomic/metabolomic molecules (e.g., proteins and lipids) that are responsible for several biological functions. In addition, they are involved in many pathological processes including cancer, neurodegeneration, cardiovascular and inflammatory diseases [7–9]. EVs released by cells into the extracellular space, or in biological fluids (e.g.,

blood, urine, saliva, breast milk) are taken up by recipient cells and deliver their functional protein and nucleic acid contents to alter the recipient cell phenotype. EVs can be utilized as diagnostic biomarkers as they act as windows of information about the cell from which they derived. EVs are also extensively used in drug delivery [10–12]. The isolation and concentration strategy of EVs used in clinical applications have strict purity requirements. Currently, EV separation methods include ultracentrifugation [13], density gradient centrifugation [14], immunochemical separation [15], size exclusion chromatography [16], membrane filtration [17] and microfluidics and microdevice-based separations [18–19]. However, there is no standard method to isolate highly pure EVs while retaining their chemical and physical properties. In selecting a separation method, one should consider the fluid type and volume from which EVs are isolated, the operational simplicity, and scalability. The technique should isolate, and concentrate pure EVs free of contaminants such as proteins and nucleic acids.

In recent studies, tangential flow filtration membrane systems were

\* Corresponding author at: National Research Council of Italy, Institute on Membrane Technology, CNR-ITM, Via P. Bucci cubo 17/C, I-87030 Rende (CS), Italy.  
E-mail addresses: [l.debartolo@itm.cnr.it](mailto:l.debartolo@itm.cnr.it), [loredana.debartolo@cnr.it](mailto:loredana.debartolo@cnr.it) (L. De Bartolo).

<https://doi.org/10.1016/j.seppur.2022.121561>

Received 14 April 2022; Received in revised form 8 June 2022; Accepted 17 June 2022

Available online 28 June 2022

1383-5866/© 2022 The Author(s). Published by Elsevier B.V. This is an open access article under the CC BY license (<http://creativecommons.org/licenses/by/4.0/>).

employed for EVs isolation and concentration [17,20]. The separation process lies in the selective transport of species promoted by a difference in chemical potential across the systems. More specifically, selective separation occurs by a size exclusion mechanism. Important parameters that influence transport across membranes include structural, physico-chemical, and permeability properties. In TFF, the fluid flow is applied tangentially to the membrane to reduce the accumulation of targeted components and filter clogging issues. However, interfacial interactions between membrane surface and molecules influence specific and non-specific binding of both target and non-target species affecting the flux and membrane performance. This often results in the presence of contaminants in the filtered solution. One strategy to overcome this limitation is to design a membrane with optimized surface properties without altering its structural properties, which are responsible for selective transport. Many efforts were devoted to exploring modification techniques aimed at introducing functional groups over the membrane surfaces to improve the separation process, avoiding the binding of contaminants and other non-target molecules. Recently, homogenous 3D polymeric coatings have been developed to modify surfaces to prevent non-specific binding while offering immobilization points for subsequent conjugation with biomolecules to facilitate the molecular recognition of a target species [21–22]. Inspired by the successful use of these polymers for microarray applications, we applied the same coating to the modification of polysulfone (PSf) membranes. PSf membranes, thanks to their chemical resistance to organic media, good thermal and mechanical stability have been used in a broad range of applications including EVs isolation and purification. Here, we propose the modification of the membrane surface by a nanometric coating of copolymers that originate from the common polymer precursor copoly-(DMA-NAS-MAPS), composed of N,N-dimethylacrylamide (DMA), 3-(trimethoxysilyl)propyl methacrylate (MAPS), and N-acryloyloxysuccinimide (NAS). We synthesized a family of polymers with different functionalities introduced by post-polymerization modification (PPM) of the parent polymer, which then enabled membrane functionalization with peptide bioprobes by click chemistry reactions. We explored the use of various polymeric coatings containing azide, benzophenone, dibenzocyclooctyne (DBCO), fluorinated groups, in different combinations and molar ratios. In our rationales, the coating has the dual purpose of limiting non-specific interactions while introducing orthogonal

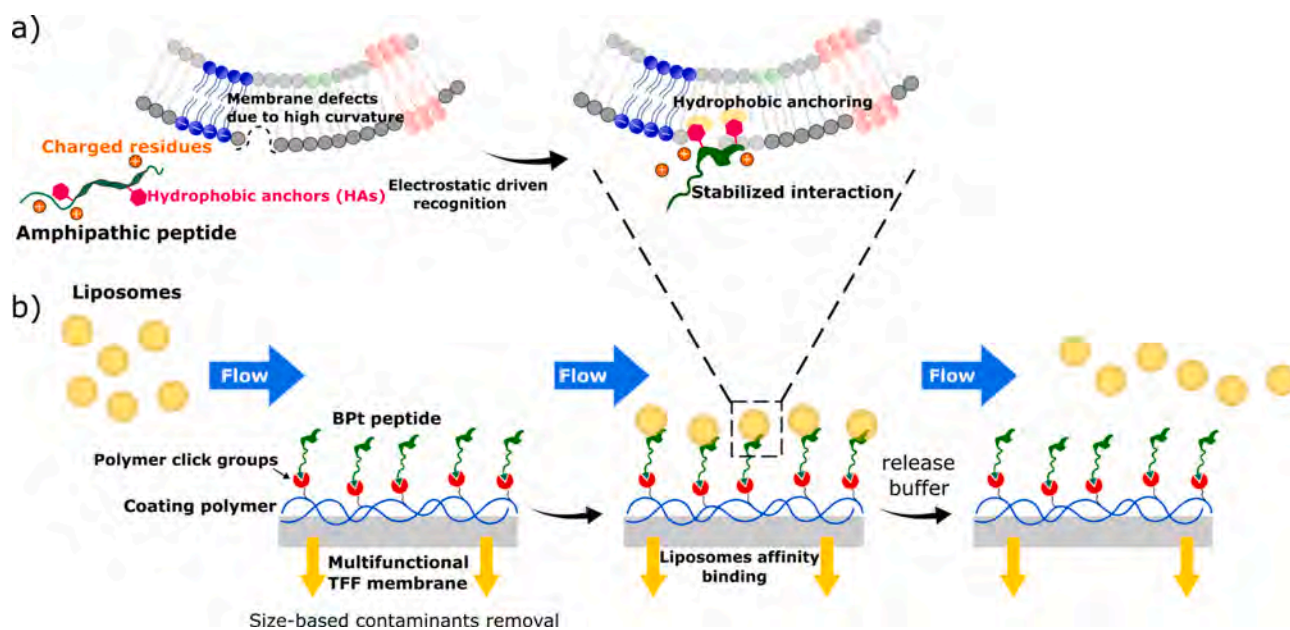
functional groups to enable the controlled conjugation of peptide ligands for lipid nanovesicle capture. Specifically, by this strategy, we set to functionalize TFF membranes with the previously reported BPT peptide (sequence: RPPGFSPFR-(O<sub>2</sub>Oc)-RPPGFSPFR-K-G-(O<sub>2</sub>Oc)<sub>2</sub>-Prg), a peptide derived from bradykinin that was shown to bind efficiently to both synthetic and biogenic lipid nanovesicles characterized by highly curved membranes (less than 150 nm), including small EVs [23]. This motif belongs to the family of membrane curvature sensing peptides (MSP), a family of peptides derived from associated curvature sensor domains in proteins [24], which selectively bind to relatively small (bio) nanovesicles through the combination of electrostatic and hydrophobic interactions. The latter “sense” lipid packing defects characteristic of highly curved and tensioned membranes (Fig. 1).

Upon membrane coating, we thoroughly investigated the homogeneity and stability of the coatings and the properties of the modified membranes, especially their ability to limit proteins’ adsorption and non-specific interactions, in comparison with the native ones. The effect of the polymeric coating on the physico-chemical properties, filtration performance and antifouling capacity of the membrane was studied. The presence of the functional groups, which are typical of the polymer used for the coating was elucidated by FT-IR spectra. The successful conjugation of the BPT peptide was also determined by confocal laser scanning microscopy and FT-IR analysis. Stability studies were performed under static and in TFF operational conditions. Finally, the membrane functionality was evaluated by assessing the capture of fluorescent liposomes in an ad-hoc designed device, which was chosen for this proof-of-concept both for the increasing importance of lipid nanoparticles in drug delivery applications and for their consolidated use as readily available surrogates of EVs. New insights on the modification of a membrane surface to reduce adsorption phenomena and to enable specific interactions with nanovesicles are emphasized in this study.

## 2. Experimental

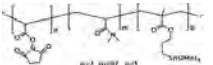
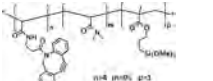
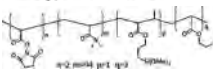
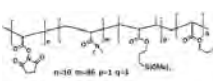
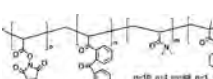
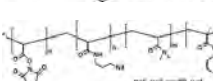
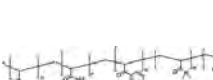
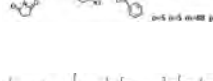
### 2.1. Copolymer synthesis and characterization

The solvents used for copolymer synthesis, such as N,N-Dimethylacrylamide (DMA), 3-(trimethoxysilyl)propyl methacrylate (MAPS), propargylamine, dibenzocyclooctyne-amine,



**Fig. 1.** Scheme of mechanism for lipidic nanovesicle capture and release: (a) amphipathic peptide approaches highly curved membranes through electrostatics, and subsequently insert into lipid-packing defects of nanovesicles, (b) functionalized membranes with BPT recognize and bind selectively liposomes during TFF and then, the liposomes bound to the membrane were released upon a treatment with divalent metal cations.

**Table 1**  
Composition, monomer fraction and chemical structures of copolymers synthesized for the membranes surface modification.

Copolymer Name	Copolymer Composition	Monomer Mole Fraction	Chemical Structure	Abbreviation
Copoly (DMA-NAS-MAPS)	dimethylacrylamide (DMA), N-acryloyloxysuccinimide (NAS), 3-(trimethoxysilyl) propyl methacrylate (MAPS)	97:2:1		c-(DMA-NAS-MAPS)
Copoly (DMA-4%DBCO-MAPS)	dimethylacrylamide (DMA), N-acryloyloxysuccinimide (NAS), 3-(trimethoxysilyl) propyl methacrylate (MAPS) where NAS is reacted with dibenzocyclooctine amine	95:4:1		c-(DMA-DBCO-MAPS)
Copoly (DMA-2%NAS-3%PFDA-MAPS)	dimethylacrylamide (DMA), N-acryloyloxysuccinimide(NAS), 1H,1H,2H,2H perfluorodecyl acrylate (PFDA), 3-(trimethoxysilyl) propyl methacrylate (MAPS)	94:2:3:1		c-(DMA-NAS-PFDA-MAPS)-1
Copoly (DMA-10%NAS-3%PFDA-MAPS)	dimethylacrylamide (DMA), N-acryloyloxysuccinimide (NAS), 1H,1H,2H,2H perfluorodecyl acrylate (PFDA), 3-(trimethoxysilyl) propyl methacrylate (MAPS)	86:10:3:1		c-(DMA-NAS-PFDA-MAPS)-2
Copoly (DMA-10% NAS-1%BP-MAPS)	dimethylacrylamide (DMA), N-acryloyloxysuccinimide (NAS), acryloyl benzophenone (BP), 3-(trimethoxysilyl) propyl methacrylate (MAPS)	88:10:1:1		c-(DMA-NAS-BP-MAPS)
Copoly (DMA-5%NAS-5%N <sub>3</sub> -MAPS)	dimethylacrylamide (DMA), N-acryloyloxysuccinimide (NAS), 3-(trimethoxysilyl) propyl methacrylate (MAPS) where 50% of the NAS monomer was reacted with 3-aminopropylazide (N <sub>3</sub> )	89:5:5:1		c-(DMA-NAS-N <sub>3</sub> -MAPS)
Copoly (DMA-5%NAS-5%N <sub>3</sub> -1%BP-MAPS)	dimethylacrylamide (DMA), N-acryloyloxysuccinimide (NAS), acryloyl benzophenone (BP), 3-(trimethoxysilyl) propyl methacrylate (MAPS) where 50% of the NAS monomer was reacted with 3-aminopropylazide (N <sub>3</sub> )	88:5:5:1:1		c-(DMA-NAS-N <sub>3</sub> -BP-MAPS)
Copoly (DMA-10%N <sub>3</sub> -1%BP-MAPS)	dimethylacrylamide (DMA), N-acryloyloxysuccinimide (NAS), acryloyl benzophenone (BP), 3-(trimethoxysilyl) propyl methacrylate (MAPS) where the NAS monomer was reacted with 3-aminopropylazide (N <sub>3</sub> )	88:10:1:1		c-(DMA-N <sub>3</sub> -BP-MAPS)

$\alpha,\alpha'$ -Azobisisobutyronitrile (AIBN), anhydrous tetrahydrofuran (THF), ammonium sulphate ( $(\text{NH}_4)_2\text{SO}_4$ ), were purchased from Sigma Aldrich (St. Louis, MO, USA). All solvents were used as received. N-acryloyloxysuccinimide and 3-azido-1-propylamine were synthesized as reported elsewhere [25–26].

Copoly (DMA-NAS-MAPS) was synthesized by free radical polymerization as previously reported [27]. Briefly, after degassing anhydrous THF with helium, DMA, NAS and MAPS were added to the reaction flask so that the total monomer feed was 20% w/v, while the molar fraction of the monomer was 97:2:1 respectively (see Table 1). The reaction mixture was heated to 65 °C for two hours in presence of  $\alpha,\alpha'$ -azobisisobutyronitrile (AIBN). The crude material was cooled to room temperature and diluted 1:1 with dry THF; the solution was then precipitated in petroleum ether (10 times the volume of the reaction mixture) to eliminate unreacted monomers. The polymer was collected by filtration as a white powder and dried under vacuum at room temperature. c-(DMA-NAS-PFDA-MAPS)-1 and c-(DMA-NAS-PFDA-MAPS)-2 were synthesized as previously reported [26]. All the monomers, DMA, NAS, MAPS and 1H,1H,2H,2H-perfluorodecyl acrylate (PFDA), were dissolved in anhydrous THF so that the total monomer feed was 20% w/v, while the molar fraction of the monomer is reported in Table 1. As previously reported, the reaction was initiated by adding AIBN and stirred at 65 °C for 2 h under inert atmosphere. After diluting the crude material 1:1 with anhydrous THF, the material was precipitated in petroleum ether and collected as a white powder. The same procedure was implemented for the synthesis of c-(DMA-NAS-BP-MAPS). In this case, the monomers added into anhydrous THF were DMA, NAS, MAPS and acryloyl Benzophenone (BP) with the molar fraction indicated in Table 1. Similarly, after 2 h reaction at 65 °C in the presence of AIBN the polymer was collected as white powder by precipitation in petroleum ether.

To introduce the azido or DBCO functionalities (c-(DMA-DBCO-MAPS), c-(DMA-N<sub>3</sub>-BP-MAPS)), a 20% w/v solution of the copolymers was prepared by dissolving it in dry THF and a 2.5 M excess with respect to the moles of NAS of the proper reagent (3-azido-1-propylamine or dibenzocyclooctyne-amine respectively) was added to the crude material, assuming that the concentration of NAS along the polymer chain is 40 mM (in a 20% w/v polymer solution). The mixture was stirred for 5 h at room temperature and then diluted 1:1 with anhydrous THF. The polymers were precipitated in petroleum ether (10 times the volume of the reaction mixture), filtered on a buchner funnel and dried under vacuum at room temperature. To further purify the obtained powder, the polymers were dissolved again in anhydrous THF to a final concentration of 10% w/v and re-precipitate in petroleum ether. The powder was finally filtered and dried again under vacuum at room temperature. Partial modification of NAS monomer of c-(DMA-NAS-N<sub>3</sub>-MAPS), c-(DMA-NAS-N<sub>3</sub>-BP-MAPS) was obtained by using 0.5 M ratio of 3-azido-1-propylamine with respect to the moles of NAS [21]. Polymers were then collected after precipitation and filtration as previously reported [22]. Copoly azide polymers were characterized by NMR. <sup>13</sup>C spectra were acquired with 600 a Bruker DRX and 400 Bruker AVANCE I spectrometers equipped with 5 mm TXI probe with z gradient and 10 mm TXI autoshimming probe, respectively. Spectra were acquired at room temperature (300 K). About 30 mg of polymer were dissolved in DMSO-*d*<sup>6</sup> solvent. Spectra were calibrated on DMSO solvent signal at 40.45 ppm.

## 2.2. Peptide synthesis and characterization

Peptide was assembled by stepwise microwave-assisted Fmoc-SPSS on a Biotage ALSTRA Initiator + peptide synthesizer, operating in a 0.05 mmol scale. Activation of entering Fmoc-protected amino acids (0.3 M solution in DMF) was performed using 0.5 M Oxyma in DMF / 0.5 M DIC in DMF (1:1:1 M ratio), with a 5-equivalent excess over the initial resin loading. Coupling steps were performed for 45 min at 50 °C. Capping steps were performed by treatment with a 0.3 M Ac<sub>2</sub>O / 0.3 M DIEA

solution in DMF (1 × 5 min). Fmoc- deprotection steps were performed by treatment with a 20% piperidine solution in DMF at room temperature (1 × 10 min). Following each coupling, capping or deprotection step, peptidyl-resin was washed with DMF (3 × 3.5 mL). Upon complete chain assembly, resin was washed with DCM (5 × 3.5 mL) and gently dried under nitrogen flow. Resin-bound peptide was treated with an ice-cold TFA, TIS, water, thioanisole mixture (90:5:2.5:2.5 v/v/v/v, 3 mL). After gently shaking the resin for 2 h at room temperature, the resin was filtered and washed with neat TFA (2 × 4 mL). Cleavage mixture was concentrated under nitrogen stream and then added dropwise to ice-cold diethyl ether (40 mL) to precipitate the crude peptide. The crude peptide was collected by centrifugation and washed with further cold diethyl ether to remove scavengers. Peptide was then dissolved in 0.1% TFA aqueous buffer (with minimal addition of ACN to aid dissolution, if necessary). Residual diethyl ether was removed by a gentle nitrogen stream. Analytical and semi-preparative reversed-phase high-performance liquid chromatography (RP-HPLC) were then carried out on a Shimadzu Prominence HPLC system equipped with a multichannel detector. A Phenomenex Jupiter 5 $\mu$  C18 90 Å column (150 × 4.6 mm) was used for analytical runs and a Phenomenex Jupiter 10 $\mu$  C18 90 Å (250 × 21.2 mm) for peptide purification. Data were recorded and processed with LabSolutions software. 5–100 % linear gradient eluent B at a flow rate of 0.5 mL/min was used for analytic purposes (20 min run). Eluent A = H<sub>2</sub>O/ 3 % CH<sub>3</sub>CN / 0.07 % TFA, eluent B = 70 % CH<sub>3</sub>CN/ 30 % H<sub>2</sub>O/ 0.07 % TFA. Peptide purification was achieved by preparative RP-HPLC at a flow rate of 14 mL/min using a 100% A → 30% B gradient over 40 min. Pure RP-HPLC fractions (>95%) were combined and lyophilized. Mass spectra were collected separately on a Shimadzu LC-MS2020 instrument. BPT HPLC trace and MS spectrum are reported in Supplementary Materials. Reagents for peptide synthesis were from Iris Biotech (Marktredwitz, Germany).

## 2.3. Liposome synthesis

Liposomes were hand extruded through a 200 nm polycarbonate membrane (Genizer Extruder). The lipid composition was set to mimic the one of EVs [28]. In details, liposomes were formulated as DOPC/SM/Chol/DOPS/DOPE at a molar ratio of 21/17.5/30/14/17.5 1,1'-Dioctadecyl-3,3,3',3'-Tetramethylindocarbocyanine Perchlorate (DiI) was included in the formulation (0.5%mol) for obtaining fluorescent liposomes. Liposomes were characterized by NTA (Nanoparticle Tracking Analysis System).

## 2.4. Surface modification of membranes

### 2.4.1. Polymer coating

PSf membranes (PALL®, Medical) were activated with a pre-treatment by dipping the surface with NaOH, 1 M for 30 min, washing accurately and then repeating the same procedure with HCl, 1 M. For the polymer coating the membranes were successively immersed for 1 h in each polymeric solution 1.5 % (w/v). All copolymers used for membrane coating, chemical composition, monomer fraction and chemical structure are reported in Table 1. Copolymers c-(DMA-NAS-N<sub>3</sub>-MAPS), c-(DMA-NAS-BP-MAPS), c-(DMA-NAS-N<sub>3</sub>-BP-MAPS), and c-(DMA-N<sub>3</sub>-BP-MAPS) were dissolved in 10% (NH<sub>4</sub>)<sub>2</sub>SO<sub>4</sub>; copolymer c-(DMA-NAS-MAPS) in 20% (NH<sub>4</sub>)<sub>2</sub>SO<sub>4</sub>. Copolymers c-(DMA-DBCO-MAPS) and c-(DMA-NAS-PFDA-MAPS)-2 were dissolved in 50% (w/v) DMF, and then diluted to the final 1.5% (w/v) in 4% (NH<sub>4</sub>)<sub>2</sub>SO<sub>4</sub>; copolymer c-(DMA-NAS-PFDA-MAPS)-1 with the same procedure but in 6% (NH<sub>4</sub>)<sub>2</sub>SO<sub>4</sub>. After the incubation time, the membranes were removed from the polymeric solution, cured at 80° C for 15 min, rinsed with distilled water, and finally dried at 40° C for 30 min.

### 2.4.2. Peptide conjugation

PSf membranes coated with copoly azide c-(DMA-NAS-N<sub>3</sub>-MAPS), c-(DMA-NAS-N<sub>3</sub>-BP-MAPS), and c-(DMA-N<sub>3</sub>-BP-MAPS) were conjugated

with BPt (RPPGFSPFR-(O<sub>2</sub>Oc)<sub>2</sub>-RPPGFSPFR-KG (O<sub>2</sub>Oc)<sub>2</sub>-Prg. Peptide was first dissolved in DMSO 10 mM stock solution and then diluted to the final concentration 150 μM in the click buffer solution (100 μM CuSO<sub>4</sub>, 400 μM THPTA, 6.25 mM ascorbic acid). Polymer-coated membranes were incubated with peptide solution overnight at RT. Thereafter, the membranes were removed from the peptide solution, rinsed twice with distilled water and dried at 37 °C for 10 min.

## 2.5. Characterization of native and functionalized membranes

### 2.5.1. Characterization of membrane properties

The morphological and structural properties of native PSf and copoly azide polymer-coated BPt conjugated membranes were evaluated by scanning electron microscope (SEM). The membrane thickness was measured with Carl Mahr 40E digital micrometer. The mean pore diameter was measured by a Capillary Flow Porometer (CFP 1500 AEXL, Porous Materials Inc., PMI, Ithaca, NY, USA). The membrane porosity was calculated by gravimetric method according to the equation (1):

$$\epsilon = \frac{W_w - W_d}{Al\rho} \times 100 \quad (1)$$

where  $W_d$  and  $W_w$  are weight of the dry and wet membranes, respectively,  $A$  is the membrane area,  $l$  is the thickness and  $\rho$  the water density. The membranes were first dried at 40 °C for 3 h and weighed, then the samples were immersed in water for 24 h and after removing fluid, by patting off the surface, were weighed. Five samples for each type of membrane were used to calculate the average value of the porosity.

The topography and roughness of native PSf and copoly azide polymer-coated BPt conjugated membranes were observed by Atomic Force Microscopy (AFM) using a Multimode 8 equipped with a Nanoscope V controller (Bruker). The AFM was operated in tapping mode to avoid sample damage with a lever oscillating at a frequency of 150 kHz (TAP150, Bruker). Images were acquired on 10x10 μm areas, with 256x256 acquisition points, and scan rate of 1 Hz. Surface roughness was estimated with respect to the mean absolute value difference,  $R_a$ , and the root mean squared difference,  $RMS$ , between the actual surface height and that of the line dividing the surface of the investigated profile into two equal areas [29].

The physico-chemical properties of the investigated membranes were characterized to evaluate their hydrophobicity/hydrophilicity by

performing water contact angle (WCA) measurements in static condition by using Contact Angle Meter, CAM 200 (KSV Instrument LTD, Helsinki, Finland).

The surface tension  $\gamma$  of the membranes and its components were calculated as function of the average values of contact angle in three different reference liquids, by application of the Good-van Oss approach [30], as previously reported [31]. In brief, the contact angle in diiodomethane, as an apolar test liquid, was used to calculate the apolar Lifshitz-van der Waals component ( $\gamma^{LW}$ ). Then, the other components of the membrane surface tension, namely acid ( $\gamma^+$ ), base ( $\gamma^-$ ) and acid-base ( $\gamma^{AB}$ ), were determined by using two polar liquids: glycerol and water. The CA in the test liquids was randomly measured on different areas of the sample surface and the results were expressed as mean  $\pm$  SEM from 10 measurements. The free energy of interfacial interaction ( $\Delta G_{iwi}$ ) between membranes (i) and water (w) was calculated by the corresponding values of  $\gamma^{LW}$ ,  $\gamma^+$ , and  $\gamma^-$  parameters, as previously reported [32].

To evaluate the stability of the improved hydrophilic character, the physico-chemical properties of PSf membranes coated with polymers containing azide group were investigated after incubation in RPMI 1640 medium (Gibco) at room temperature. After 1, 2 and 3 h within the medium, samples were dried at 40 °C and the WCA was measured.

FT-IR spectra were recorded on native and on all polymer-coated and peptide-conjugated membranes by a Perkin Elmer precisely FT-IR Spectrophotometer, and analysed using the Spectrum One software (Perkin Elmer). The spectra were recorded over the 4000–400  $\text{cm}^{-1}$  wave number range.

The convective transport of solutes through the membrane is determined by the membrane hydraulic permeance  $L_p$ , evaluated from filtration flux in the absence of solutes and at different transmembrane pressures ( $\Delta P^{TM}$ ) [33]. A cell filtration unit in which the flat-sheet membrane is located was setup and connected to a peristaltic pump that fed pure water to the inlet port of the cell. Pressures were monitored at inlet and outlet of the cell by online manometers (Allemano, accuracy  $\pm$  0.98 mbar). Inlet pressure were varied from 10 to 200 mbar and permeate was measured continuously at increasing transmembrane pressure. The hydraulic permeance  $L_p$  was estimated by applying eq. (2) in which a linear dependency between water flux and the convective driving force is expressed:

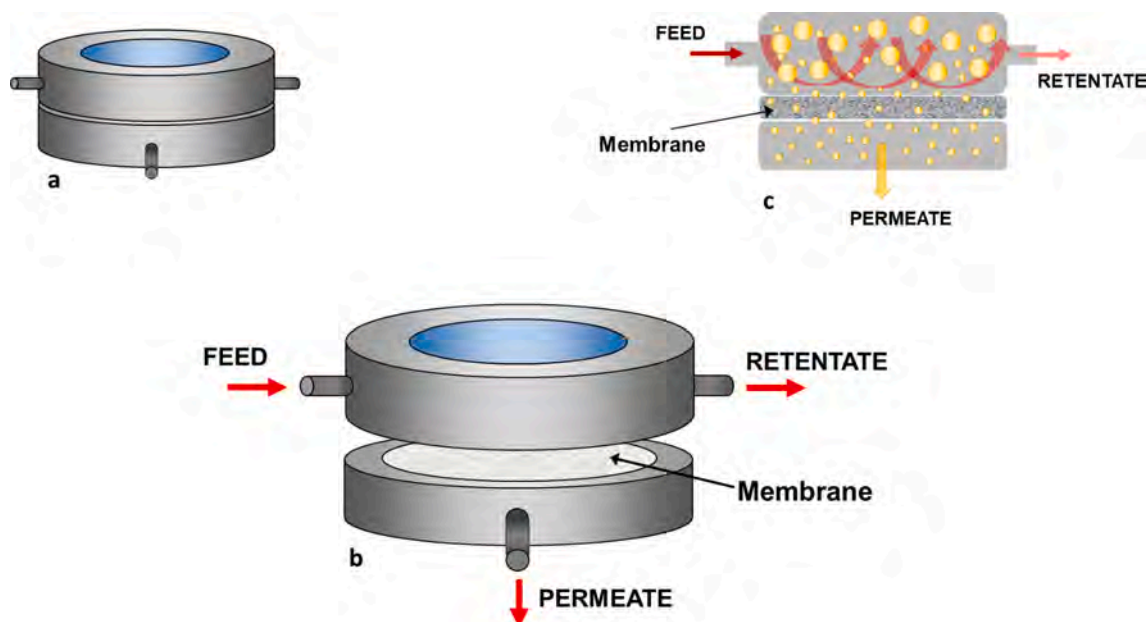


Fig. 2. TFF cell unit closed (a) and opened with membrane housing (b). Scheme of the separation process of the tangential flow filtration or cross-flow filtration (c).

$$L_P = \left( \frac{J_{Solvent}}{\Delta P_{TM}} \right)_{\Delta c=0} \quad (2)$$

### 2.5.2. Quantification of conjugated peptide

The amount of peptide conjugated with click reaction on PSf copoly azide polymer-coated membranes was quantified by Bicinchoninic Acid Quanti Pro Assay (Sigma Aldrich). Moreover, peptide conjugation on PSf copoly azide polymer-coated membranes was assessed by confocal laser scanning microscopy (CLSM) after click reaction with peptide FITC-conjugated. The stability of the peptide conjugation was assessed by qualitative and quantitative CLSM analysis, after the membrane modification (time 0), after 1, 2 and 3 h of medium immersion in static condition, and after 1.5 h of medium tangential flow filtration (TFF).

## 2.6. Tangential flow filtration (TFF)

### 2.6.1. TFF cell unit

The unit for TFF consists of a still cell with two compartments separated by the section for the membrane housing (Fig. 2). The upper

compartment is fitted with an inlet port for the feeding of solutions to be filtered. Two outlet ports, in the upper and lower compartments allow the retentate and permeate collection, respectively. TFF, also known as *cross-flow filtration*, is a process of separation in which the particles that pass through the membrane, the permeate, are put off to the side, while the rest, the retentate, is cut off and recycled back to the feed. The total volume of the cell units is 4 cm<sup>3</sup> and the membrane surface area 3.97 cm<sup>2</sup>. For TFF the cell unit was connected to a perfusion system consisting of tubes and peristaltic pump that ensures a constant flow rate.

### 2.6.2. Membrane filtration

PSf membrane before (native) and after the coating with copoly azide polymers c-(DMA-NAS-N<sub>3</sub>-MAPS), c-(DMA-NAS-N<sub>3</sub>-BP-MAPS), and c-(DMA-N<sub>3</sub>-BP-MAPS) were used in TFF to assess their fouling after filtration of protein solution. To this purpose a solution of 5% foetal bovine serum (FBS) in phosphate buffered saline (PBS) at a flow rate of 1.6 mL/min for 120 min was fed to the cell unit. The permeate volume was collected during the time with respective feed and retentate. The flow rate (*J*) was calculated as [L/m<sup>2</sup> h]. Antifouling properties of PSf

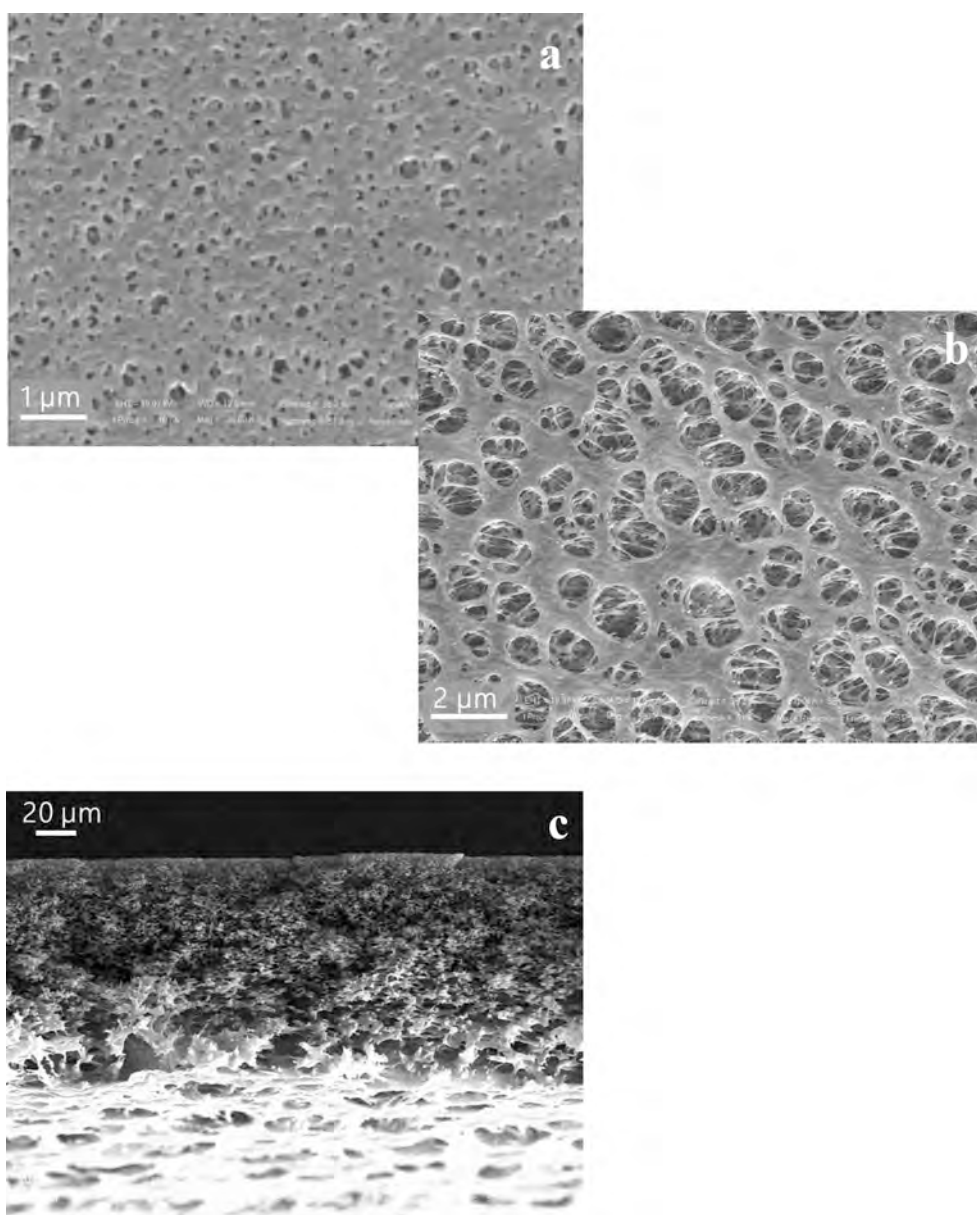


Fig. 3. SEM images of the surface (a-b) and cross section (c) of PSf membrane.

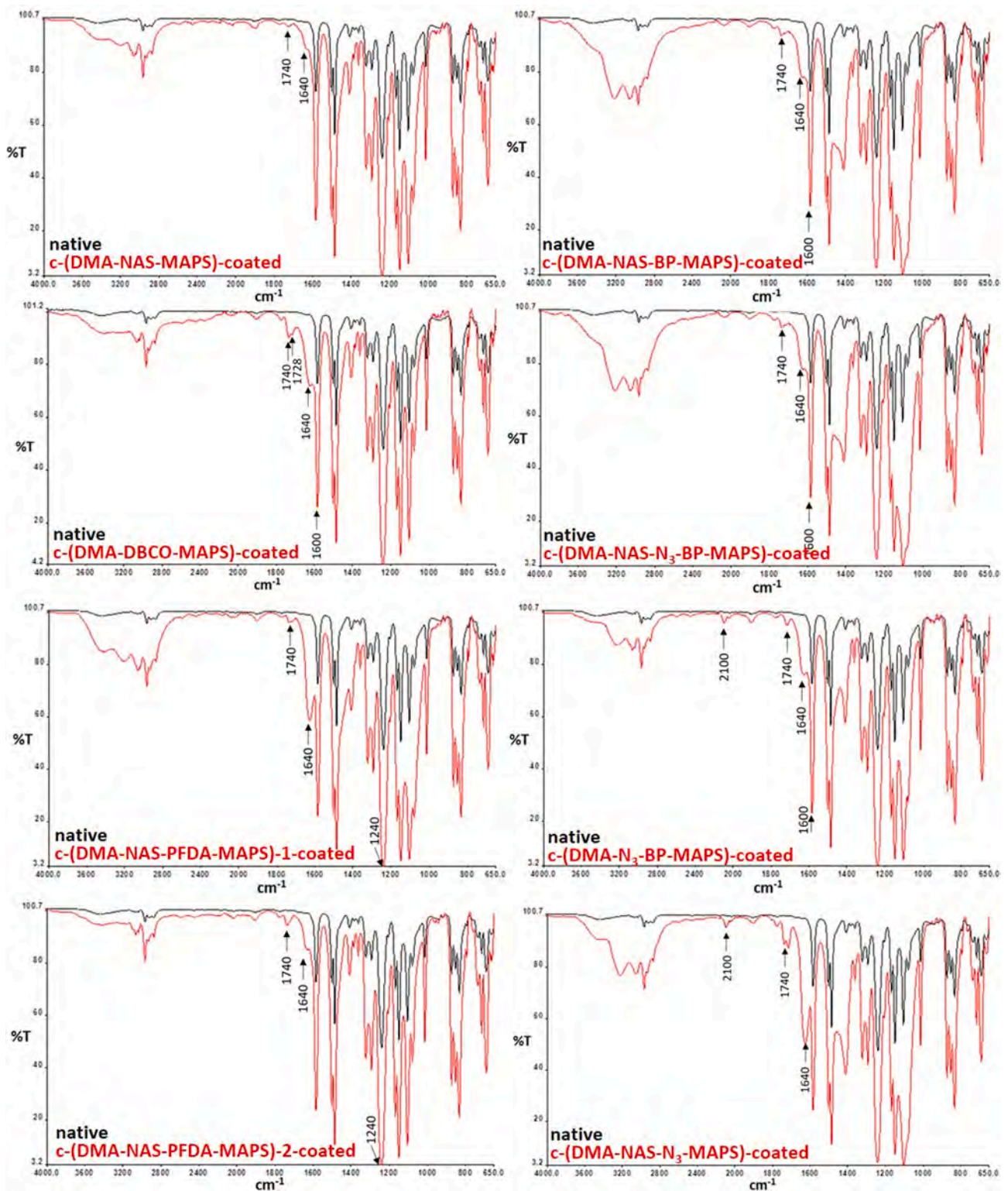


Fig. 4. FT-IR spectra of the native and copolymer coated membranes. Characteristic peaks of the different functionalities illustrate modifications made to the membrane surface.

copoly azide polymers-coated membranes were assessed by the quantifying the concentration of proteins adsorbed on the membrane, and present in permeate and feed and retentate solutions, by BCA Assay. Initial permeate flux ( $J_0$ ), permeate flux after fouling ( $J_1$ ) and permeate flux after cleaning and washing ( $J_2$ ) were recorded to evaluate flux decline ratio (FDR) and flux recovery ratio (FRR) through the eq. (3) and eq. (4), respectively:

$$FDR = \left(1 - \frac{J_1}{J_0}\right) \times 100 \quad (3)$$

$$FRR = \frac{J_2}{J_0} \times 100 \quad (4)$$

For the fouling analysis membrane filtration resistance ( $R_m$ ), reversible fouling resistance  $R_r$  and irreversible fouling resistance ( $R_{ir}$ ) were calculated by Darcy's law:

$$J = \frac{\Delta P}{\mu R_t} \quad (5)$$

where  $J$  is the permeation flux of solution ( $\text{m}^3/\text{m}^2\text{s}$ ),  $\Delta P$  is the transmembrane pressure (Pa);  $\mu$  is the dynamic viscosity (Pa s);  $R_t$  is the total resistance ( $\text{m}^{-1}$ ) and it is given:

$$R_t = \frac{\Delta P}{\mu J} = R_m + R_r + R_{ir} \quad (6)$$

( $R_m$ ) is the intrinsic resistance characteristic of membrane properties;  $R_{re}$  and  $R_{ir}$  are reversible resistance and irreversible resistance, respectively. The resistances of membranes were calculated according to the following equations [34]:

$$R_m = \frac{\Delta P}{\mu J_0} \quad (7)$$

$$R_t = \frac{\Delta P}{\mu J_p} \quad (8)$$

$$R_{ir} = \frac{\Delta P}{\mu J_c} - R_m \quad (9)$$

$$R_r = \frac{\Delta P}{\mu J_p} - \frac{\Delta P}{\mu J_c} \quad (10)$$

where  $J_0$  is the pure water flux of new membrane,  $J_p$  is the flux after the FBS filtration,  $J_c$  is the pure water flux of the fouled membrane after surface rinsing and  $\mu$  is water viscosity.

### 2.6.3. TFF for liposome capture and release

The capacity of c-(DMA-N<sub>3</sub>-BP-MAPS)-BPT conjugated membrane to capture liposomes in TFF was assessed and compared to the PSf-BPT adsorbed and native membranes. Fluorescent liposomes (10 mL, 10<sup>9</sup> part/mL) were flowed in the TFF cell unit loaded with modified and native membranes at 4 °C for 30 min, with a flow rate of 0.5 mL/min under a recycle mode. Liposomes in the feed, retentate and permeate solutions, and on the investigated membranes after the TFF process, were observed by CLSM. The captured liposomes were successfully released by treatment with MgCl<sub>2</sub> (10 mM). Fluorescence intensity of liposomes captured by the BPT-modified functionalized membrane was compared with the residual fluorescence of the membrane upon MgCl<sub>2</sub> incubation.

## 3. Results and discussion

### 3.1. Effect of coating on membrane properties

The structure of the synthetic polymers (Table 1) used for membrane functionalization were previously characterized by NMR in order to confirm the insertion of the different moieties (e.g., azide, benzophenone, dibenzocyclooctine (DBCO), and fluorinated groups) in comparison with parent polymer precursor c-(DMA-NAS-MAPS) [21–22]. New insights into NMR spectra related to c-(DMA-NAS-N<sub>3</sub>-MAPS), c-(DMA-N<sub>3</sub>-BP-MAPS), c-(DMA-NAS-N<sub>3</sub>-BP-MAPS) show the most indicative signals belonging to the carbonyl zone between 168 and 176 ppm. In this region, it is possible to observe two peaks belonging to the carbonyls of succinimidyl moiety at 174 and 171 ppm whose integrals decrease in the c-(DMA-NAS-N<sub>3</sub>-MAPS) spectrum and totally disappear in the c-(DMA-N<sub>3</sub>-BP-MAPS) spectrum. In c-(DMA-NAS-N<sub>3</sub>-MAPS), c-(DMA-N<sub>3</sub>-BP-MAPS), an additional signal at 172.3 ppm, corresponding to the

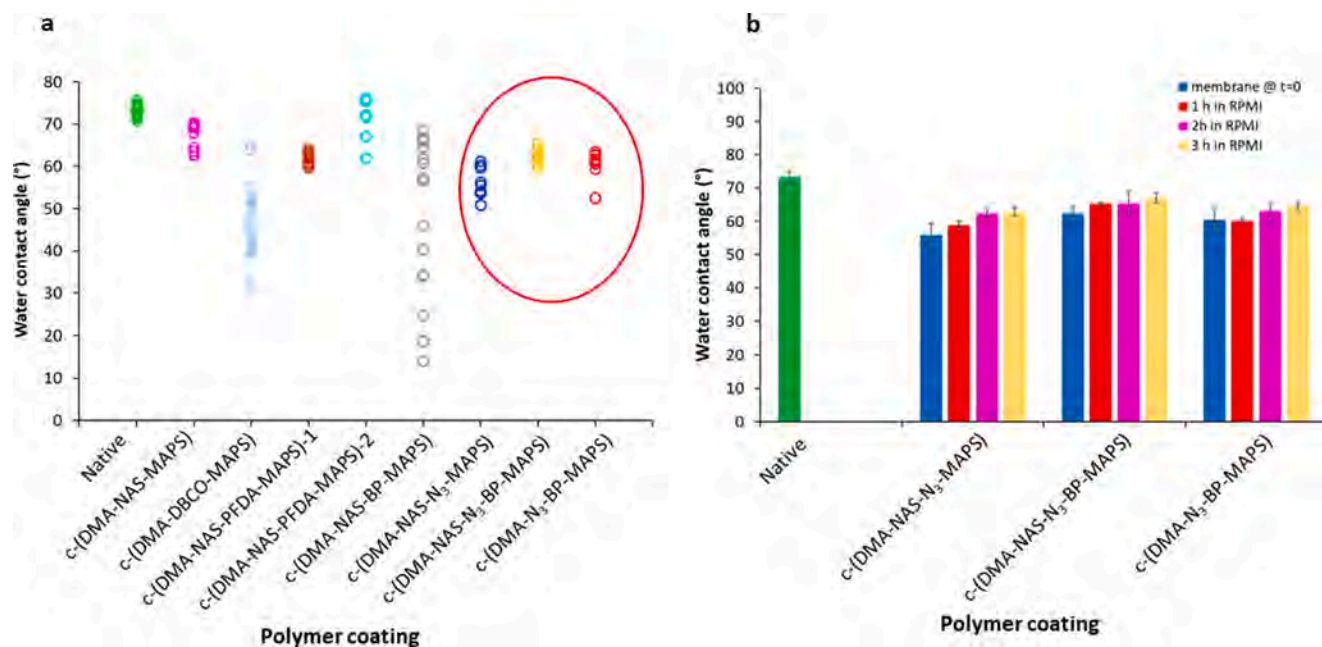


Fig. 5. Water contact angle values of membranes coated with different copolymers in comparison with the native one (a); wettability of copoly azide polymers coated membranes in comparison with the native one after incubation at different time in RPMI medium (b).



**Table 2**

Physico-chemical properties of native and copoly azide polymer coated membranes. Contact angles ( $\theta$ ) in water (W), glycerol (Gly), diiodomethane (DIM); Lifshitz-van der Waals ( $\gamma^{LW}$ ), acid ( $\gamma^+$ ), base ( $\gamma^-$ ), acid-base ( $\gamma^{AB}$ ) components of the surface tension ( $\gamma$ ) of the membranes that were calculated according to Good-van Oss equation by the average values of measured contact angle values; ( $\Delta G_{iwi}$ ) free energy of interfacial interaction between membrane (i) and water (w).

MEMBRANE	$\theta_w$ [°]	$\theta_{Gly}$ [°]	$\theta_{DIM}$ [°]	$\gamma^{LW}$ [mJ/m <sup>2</sup> ]	$\gamma^+$ [mJ/m <sup>2</sup> ]	$\gamma^-$ [mJ/m <sup>2</sup> ]	$\gamma^{AB}$ [mJ/m <sup>2</sup> ]	$\gamma$ [mJ/m <sup>2</sup> ]	$\Delta G_{iwi}$ [mJ/m <sup>2</sup> ]
Native PSf	73.3 ± 1.6	86.1 ± 1.7	27.3 ± 2.5	45.3	3.9	25.4	20.0	65.3	-8.6
c-(DMA-NAS-N <sub>3</sub> -MAPS)-coated	54.7 ± 3.7	71.9 ± 1.9	38.4 ± 1.9	40.4	1.2	43.1	14.1	54.0	18.6
c-(DMA-NAS-N <sub>3</sub> -BP-MAPS)-coated	58.8 ± 2.4	72.9 ± 0.7	37.7 ± 1.8	40.7	1.1	36.9	12.6	53.3	10.6
c-(DMA-N <sub>3</sub> -BP-MAPS)-coated	61.6 ± 1.9	77.0 ± 2.3	37.6 ± 1.6	40.8	1.8	36.7	16.1	56.0	9.1

carbonyl amide of the linker bearing the azide moiety, appears. In the aromatic region, between 128 and 139 ppm, the four signals of the BP aromatic ring are detected only in the polymers containing the BP monomer, as well as its carbonyl atom at 195.4 ppm.

The structural, physico-chemical, and permeability properties of membranes were characterized before and after the modification process to evaluate changes of their properties due to the surface functionalization. Representative SEM micrographs reported in Fig. 3 show the morphological structure of the native PSf membranes characterized by a homogeneous microporous surface with a mean pore diameter of  $0.16 \pm 0.031 \mu\text{m}$ , revealed by flow porometer investigation. The cross-section in Fig. 3C highlights the asymmetric porous structure of the membranes with a thickness of  $129.7 \pm 0.96 \mu\text{m}$ . Since the convective

transport of solutes through the membrane is determined by the hydraulic permeance  $L_p$ , we evaluated this parameter from filtration flux in the absence of solutes and at different transmembrane pressures ( $\Delta P^{\text{TM}}$ ). Native membranes display a hydraulic permeance  $L_p$ , of  $9.19 \text{ L/m}^2 \text{ h mbar}$ , with a R-squared value of 0.9875.

The presence of the various copolymer coatings of the membrane surfaces was confirmed by FT-IR spectroscopy. Spectra of all modified membranes compared to the native membrane, show new peaks associated with the specific copolymer functionalities corroborating the surface functionalization of the PSf membrane (Fig. 4). The coating with polymer c-(DMA-NAS-MAPS), the parent polymer, shows a typical peak at  $1740 \text{ cm}^{-1}$  corresponding to the stretching of C=O esters in N-acryloyloxysuccinimide (NAS) and 3-(trimethoxysilyl) propyl

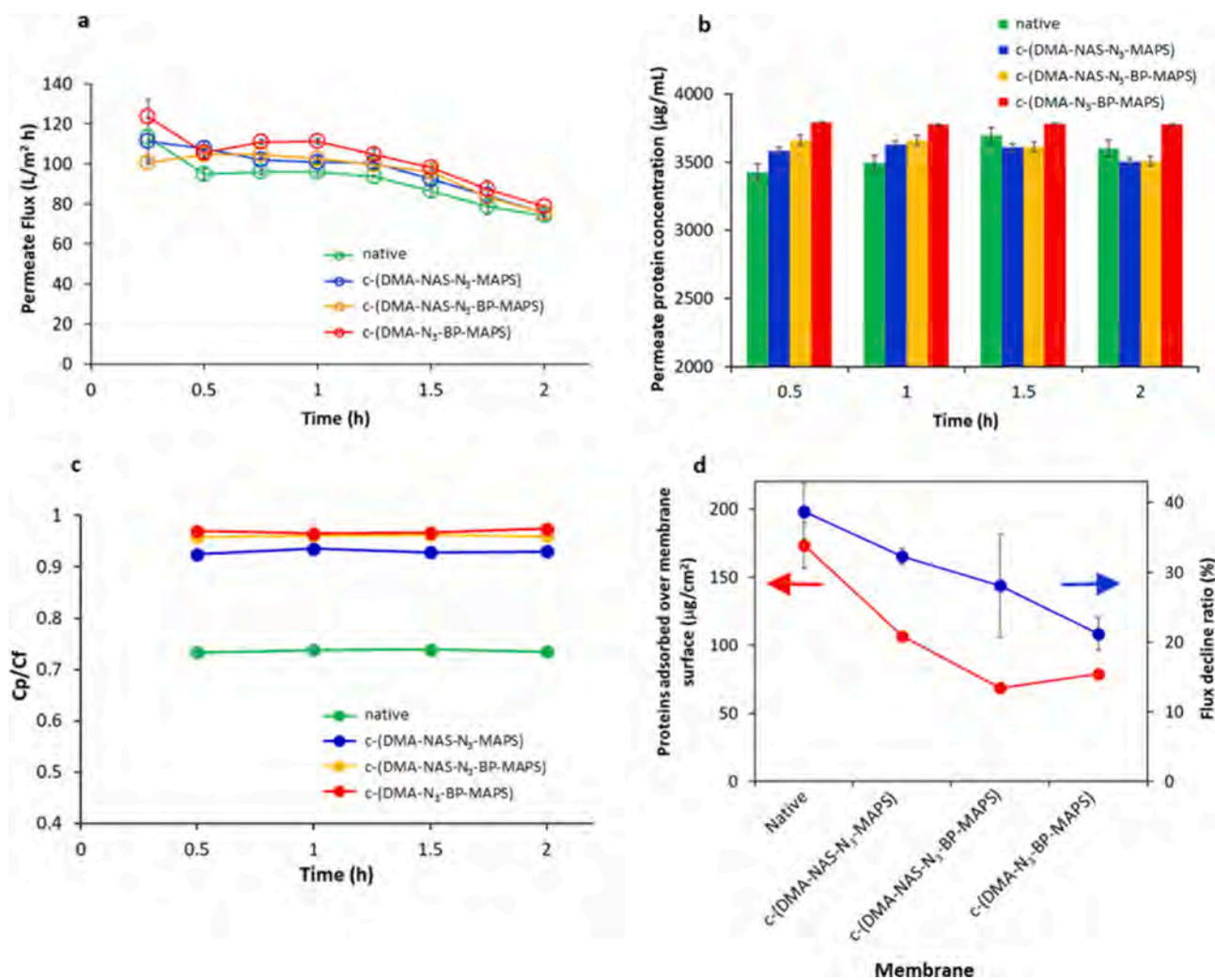


**Fig. 6.** Influence of the copolymer coating on the antifouling capacity of membranes. a) Changes of permeate flux, b) permeate protein concentration with time, c) ratio from protein permeate concentration ( $C_p$ ) to the respective feed concentration ( $C_f$ ), d) flux decline ratio and amount of proteins adsorbed over modified membranes with copolymers in comparison with native one.

methacrylate (MAPS), and a peak at  $1640\text{ cm}^{-1}$ , which corresponds to the stretching of the C=O of amide in the N,N-dimethylacrylamide (DMA). In addition to these peaks, which appear in each spectrum of all the copolymer-coated membranes, typical signals of the introduced functional groups are evident.

A peak at  $1728\text{ cm}^{-1}$  of the Dibenzocyclooctyne (DBCO) group with strong band at  $1635\text{ cm}^{-1}$  based on the C=C stretching vibration of its aromatic ring is evident in the spectrum of the membrane coated with c-(DMA-DBCO-MAPS). In the spectra of membranes coated with c-(DMA-NAS-PDFA-MAPS)-1 and c-(DMA-NAS-PDFA-MAPS)-2 the C-F stretching at  $1240\text{ cm}^{-1}$  shows a strong absorption overlapped with  $\text{CH}_2$  wagging. Adsorption peaks at  $1600\text{ cm}^{-1}$  corresponding to the ketonic C=O group, which is distinctive band belonging to benzophenone, are evident in the spectra of membranes coated with the copolymers c-(DMA-NAS-BP-MAPS), c-(DMA-NAS- $\text{N}_3$ -BP-MAPS) and c-(DMA- $\text{N}_3$ -BP-MAPS). Moreover, the typical peak of the azide group at  $2100\text{ cm}^{-1}$  appears in the spectra of membranes coated with copoly azide polymers c-(DMA-NAS- $\text{N}_3$ -MAPS), c-(DMA-NAS- $\text{N}_3$ -BP-MAPS) and c-(DMA- $\text{N}_3$ -BP-MAPS).

Coated membranes, analysed through contact angle measurements, feature different wettability, as reported in Fig. 5a. The native membrane exhibits a moderate surface wettability with water contact angle (WCA) values of  $73 \pm 1.6^\circ$ . Overall, the different copolymer coatings, owing to their hydrophilic character, influence the physico-chemical properties of the native membrane inducing a decrease in water contact angle values (Fig. 5a). In the case of c-(DMA-NAS-PDFA-MAPS)-2 and c-(DMA-NAS-MAPS) values of  $71.5 \pm 4.4^\circ$  and  $67.5 \pm 3.4^\circ$  were obtained. This minimal decrease in WCA suggests that such polymers do not have a significant influence on material hydrophilicity. A significant variation of contact angles was observed with polymers c-(DMA-DBCO-MAPS) and c-(DMA-NAS-BP-MAPS) with a wide range of values from  $31^\circ$  to  $65^\circ$  and from  $19^\circ$  to  $69^\circ$ , respectively. Nevertheless, in this case, the obtained results revealed a heterogeneity of the coated surface probably due to the weak interactions between polymer and membrane. On the other hand, the contact angles of membranes modified with copolymers c-(DMA-NAS-MAPS), c-(DMA-NAS-PDFA-MAPS)-1, c-(DMA-NAS- $\text{N}_3$ -BP-MAPS) and c-(DMA- $\text{N}_3$ -BP-MAPS), decrease significantly to average values of  $54.7 \pm 3.7^\circ$ ,  $60.5 \pm 0.3^\circ$ ,  $58.8 \pm 2.4^\circ$  and  $61.6 \pm 1.9^\circ$ , respectively. These values were reliable, repeatable and stable over time. On the basis of these findings and considering that copoly azide polymers enable the conjugation of the azide moiety with peptide BPt, the copolymers c-(DMA-NAS- $\text{N}_3$ -MAPS), c-(DMA-NAS- $\text{N}_3$ -BP-MAPS), and c-(DMA- $\text{N}_3$ -BP-MAPS), which have displayed a marked

and stable wettability feature, were further investigated to establish the surface free energy parameters. It should be considered that membranes modified with the various copolymers can exhibit different polar and apolar characteristics. The Lifshitz–Van Der Waals ( $\gamma^{\text{LW}}$ ), acid ( $\gamma^+$ ), base ( $\gamma^-$ ) and acid–base ( $\gamma^{\text{AB}}$ ) components of surface tension, were calculated by contact angle measurements in three different reference liquids, according to Good and van Oss' approach [30] and the data are reported in Table 2. The polymer coating significantly modified the values of both contact angles and surface tension components. The contact angle in water and glycerol of the native membranes ( $\theta_{\text{W}}: 73.3 \pm 1.6^\circ$ ;  $\theta_{\text{Gly}}: 86.1 \pm 1.7^\circ$ ) significantly decreased with the coating of c-(DMA-NAS- $\text{N}_3$ -MAPS) ( $\theta_{\text{W}}: 54.7 \pm 3.7^\circ$ ;  $\theta_{\text{Gly}}: 71.9 \pm 1.9^\circ$ ), c-(DMA-NAS- $\text{N}_3$ -BP-MAPS) ( $\theta_{\text{W}}: 58.8 \pm 2.4^\circ$ ;  $\theta_{\text{Gly}}: 72.9 \pm 0.7^\circ$ ) and c-(DMA- $\text{N}_3$ -BP-MAPS) ( $\theta_{\text{W}}: 61.6 \pm 1.9^\circ$ ;  $\theta_{\text{Gly}}: 77.0 \pm 2.3^\circ$ ); while the values in diiodomethane  $\theta_{\text{DIM}}$  ( $27.3 \pm 2.5^\circ$ ) increased to values of  $38.4 \pm 1.9^\circ$ ;  $37.7 \pm 1.8^\circ$ , and  $37.6 \pm 1.6^\circ$ , respectively. The coating of native membrane with the three selected copolymers produced a decrease of  $\gamma^{\text{LW}}$  value indicating a reduction of the apolar properties of the membrane since a surface features a higher hydrophobicity on account of the LW character that it exhibits, together with having little Lewis acid or Lewis base character. Importantly, the base component  $\gamma^-$ , which is representative of the hydrophilic character of surface, significantly increases after the coating with the copolymers compared to the native membrane. Surfaces coated with the copolymers c-(DMA-NAS- $\text{N}_3$ -MAPS), c-(DMA-NAS- $\text{N}_3$ -BP-MAPS), and c-(DMA- $\text{N}_3$ -BP-MAPS) display electron donor component ( $\gamma^-$ ) values of 43.1, 36.9 and  $36.7\text{ mJ/m}^2$ , respectively. These findings clearly indicate that the coating with these polymers deeply enhances the Lewis-base sites over the membrane. To further investigate the hydrophobic/hydrophilic character of native and modified membranes, the free energy of interfacial interaction ( $\Delta G_{\text{iwi}}$ ) between membrane (i) and water (w), was calculated.

Native PSf membranes have a negative value of  $\Delta G_{\text{iwi}}$  ( $-8.6\text{ mJ/m}^2$ ) that suggests its low affinity for water. In the case of modified membranes, their free energy of interaction is repulsive as indicated by the positive values of  $\Delta G_{\text{iwi}}$  reported in Table 2. These membranes have a higher affinity to water and are more hydrophilic than the native ones. The more positive the  $\Delta G_{\text{iwi}}$  the more hydrophilic is the membrane.

The stability of the coating would broadly impact the performance of the membranes. To ascertain the stability, the physico-chemical properties of the membranes coated with copoly azide polymers were evaluated after incubating the membranes for different times in the culture medium RPMI (Fig. 5b). Only a slight and negligible increase of WCA values was observed overtime for each copolymer coating due to

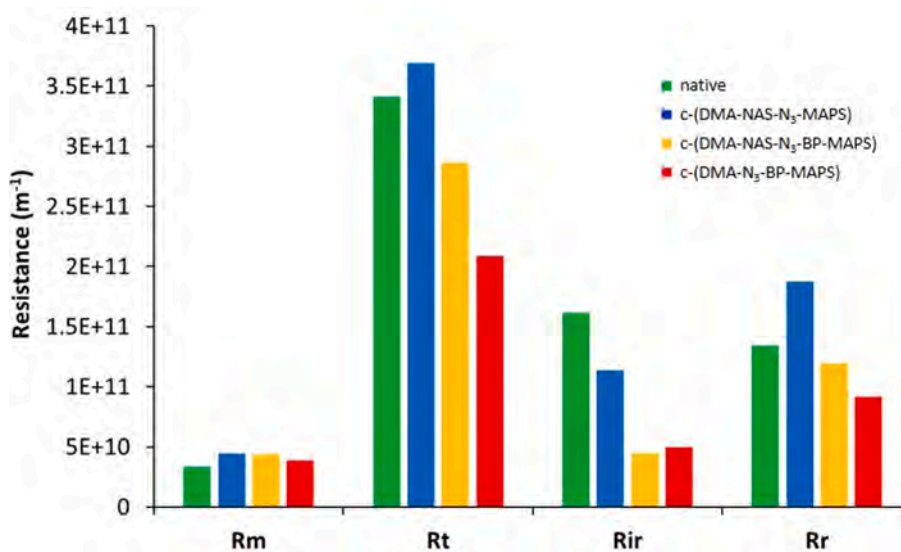
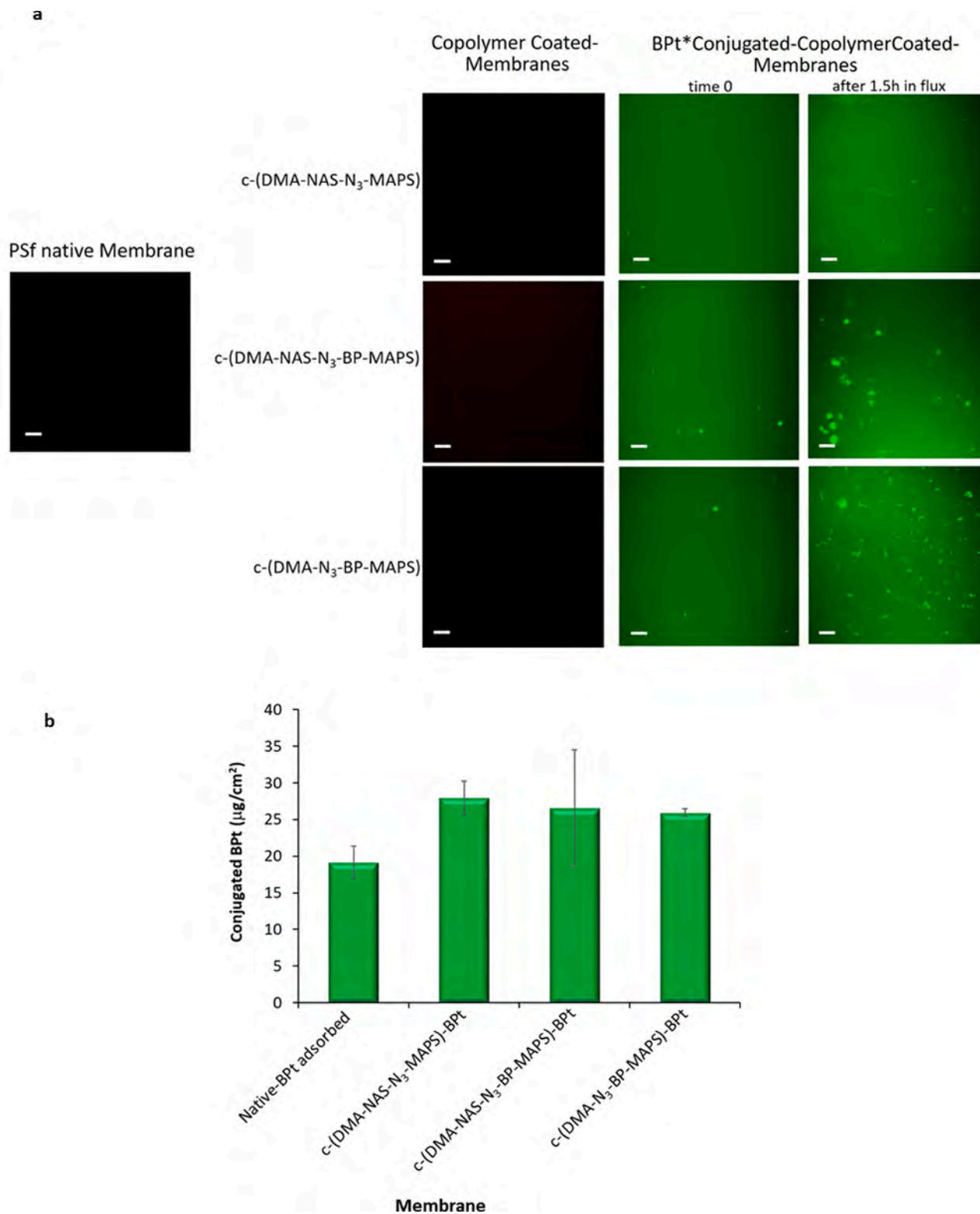


Fig. 7. Variation in membrane fouling resistances of native and copoly azide polymer coated membranes.

adsorption phenomena that can occur over the membrane surface. Indeed, after 3 h within the medium WCA was  $63.2 \pm 1.3^\circ$  for membranes coated with c-(DMA-NAS-N<sub>3</sub>-MAPS),  $67.1 \pm 1.5^\circ$  with c-(DMA-NAS-N<sub>3</sub>-BP-MAPS) and  $64.7 \pm 1.3^\circ$  with c-(DMA-N<sub>3</sub>-BP-MAPS). In any case, the WCA values are lower than native membranes. These data

suggest that wettability features of the modified membranes remain stable with time.



**Fig. 8.** CLSM images of membranes functionalized with BPT-Fluo\* (green) at time 0 and after 1.5 h of medium tangential flow in comparison with the copoly azide polymer coated and native membranes; scale bar 20 µm (a). Amount of BPT conjugated on copoly azide polymer-coated membranes and adsorbed on the native one (b).

### 3.2. Filtration performance and antifouling capacity of copolymer coated membranes

One of the main challenges of the membrane filtration process especially for vesicles isolation is to reduce contaminants including proteins, nucleic acids etc., that interfere with the separation process and purity of the product. To elucidate this issue, we investigated the filtration performance and antifouling capacity of membranes coated with the copoly azide polymers in comparison with the native one. Experiments were performed under tangential flow filtration condition established by using the device as previously described (Fig. 2). Fig. 6a shows the membrane permeate flux obtained by filtering a solution containing FBS. A slow reduction of permeate flux with time is observed for all membranes owing to protein adsorption on the membrane surface. However, the reduction is minimal with coated membranes, especially in the case of the membrane coated with c-(DMA-N<sub>3</sub>-BP-MAPS) due to the coating ability to reduce protein adsorption. Indeed, a greater protein concentration in the permeate was measured for this membrane (Fig. 6b). A noticeable increase of the ratio of protein permeate concentration (C<sub>p</sub>) to the respective feed concentration (C<sub>f</sub>) was observed for the modified membranes (Fig. 6c) displaying a low fouling tendency. This ratio reached values of about 0.97 on c-(DMA-N<sub>3</sub>-BP-MAPS) coated membranes demonstrating that proteins freely pass across the membrane.

Consistent with the protein filtration result is the flux decline ratio, which was calculated through eq. (3). The membrane fouling originates from the interaction between membrane surface and proteins that adsorb over the surface causing the flux decline that is higher for the native membranes with respect to the modified ones (Fig. 6d). The flux decline ratio decreased from  $38.7 \pm 3.9\%$  to  $21.2 \pm 2.4\%$  after coating the membrane with c-(DMA-N<sub>3</sub>-BP-MAPS) highlighting its capability to reduce protein adsorption. The decrease of flux is related to the amount of protein adsorbed over the membrane surface. We found the highest protein density on the native membrane surface ( $173.5 \pm 16.6 \mu\text{g}/\text{cm}^2$ ). The coating with copolymers reduces the fouling as demonstrated by the significant decrease of proteins adsorption on modified membranes reaching the lowest values on c-(DMA-N<sub>3</sub>-BP-MAPS) membrane surface (Fig. 6d). The amount of protein adsorbed over the membrane is determined by its surface properties and on the free energy of interfacial interaction  $\Delta G_{\text{iwi}}$ . The membranes coated with the copolymers display a positive value of  $\Delta G_{\text{iwi}}$  differently from the native one where a greater number of adsorbed proteins was measured after 2 h of TFF. This correlates well with the reduction in protein adsorption that was observed for all modified membranes. However, it is important to notice that the observed adsorption phenomenon is related also to protein physico-chemical properties [33,35]. In these experiments we used serum that contains a mix of proteins with different hydrophilic/hydrophobic character, therefore their interaction with the membrane surface is influenced by their different affinity for the surface, bulk concentration, diffusion rate as well as structural rigidity.

For further assessing the fouling behaviour of the membranes we compared the membrane resistances R<sub>m</sub>, R<sub>t</sub>, R<sub>ir</sub> and R<sub>r</sub> (Fig. 7). It can be noted that all membranes retained a relatively low R<sub>m</sub>. For native membrane the most significant resistances were both R<sub>ir</sub> ( $1.74 \times 10^{11} \text{ m}^{-1}$ ) and R<sub>r</sub> ( $1.34 \times 10^{11} \text{ m}^{-1}$ ) especially R<sub>ir</sub> that contributed to large extent of the total resistance. The modification process brought a

reduction in irreversible fouling component that ranged from  $1.23 \times 10^{11} \text{ m}^{-1}$  to  $6.86 \times 10^{10} \text{ m}^{-1}$  particularly for c-(DMA-NAS-N<sub>3</sub>-MAPS) membranes that displayed the lowest value of R<sub>ir</sub>. The reversible fouling resistances changes were consistent with R<sub>t</sub> values for the membranes coated with copoly azide polymers. In particular, the reversible component of the fouling resistance was more dominant with respect to the irreversible component that was even lower than the reversible component. The flux recovery ratio was about of 84% in the case of c-(DMA-NAS-N<sub>3</sub>-MAPS) membrane (Table S1).

### 3.3. Peptide functionalization

PSf membranes coated with copoly azide polymers c-(DMA-NAS-N<sub>3</sub>-MAPS), c-(DMA-NAS-N<sub>3</sub>-BP-MAPS), and c-(DMA-N<sub>3</sub>-BP-MAPS) were functionalized by click chemistry reaction, enabling the conjugation of the azide moiety with peptide Bpt (RPPGFSPFR-(O<sub>2</sub>C)<sub>2</sub>-RPPGFSPFR-KG (O<sub>2</sub>C)<sub>2</sub>-Prg). The peptide was in-house synthesized, isolated by RP-HPLC purification and analysed by mass spectrometry for identity confirmation (Figs. S1 and S2). The effective functionalization of membrane surfaces with the peptide was evaluated by FT-IR analysis. The typical peak of the azide group at  $2100 \text{ cm}^{-1}$  found in the FT-IR spectra difference between the native and the c-(DMA-N<sub>3</sub>-BP-MAPS)-Bpt coated membrane, disappears in the spectra difference between the functionalized c-(DMA-N<sub>3</sub>-BP-MAPS)-Bpt and the c-(DMA-N<sub>3</sub>-BP-MAPS) confirming the peptide binding with the polymer azide moiety via click reaction (Fig.S3). The homogeneity and distribution of the peptide bound to the membrane surface was evaluated by confocal laser scanning microscopy by using a FITC-conjugated peptide (Fig. 8a). After the click reaction, a bright homogeneous green fluorescence was visualized on the surface of the copoly azide polymer-coated membranes, demonstrating the functionalization of membranes with the FITC-labelled peptide. No differences were observed among the different copoly azide polymer coated membranes after conjugation (time 0) and after 1.5 h under flux conditions, as a demonstration of the immobilized peptide bond stability. These results are corroborated by a quantitative analysis of the peptide conjugated with the azide moiety of the copolymers-coated membranes that ranged from 26 to  $28 \mu\text{g}/\text{cm}^2$  (Fig. 8b). We found a similar amount of conjugated peptide over membranes modified with the different copolymers:  $26.6 \pm 7.9 \mu\text{g}/\text{cm}^2$  for c-(DMA-NAS-N<sub>3</sub>-MAPS),  $27.9 \pm 2.3 \mu\text{g}/\text{cm}^2$  for c-(DMA-NAS-N<sub>3</sub>-BP-MAPS), and  $25.9 \pm 0.5 \mu\text{g}/\text{cm}^2$  for c-(DMA-N<sub>3</sub>-BP-MAPS) membranes. These results confirm that the chemoselective conjugation of peptide over polymer coated surface via click chemistry reaction is effective and reproducible which is crucial for vesicles recognition and capture. Differently, the amount of peptide adsorbed to the native membrane surface through non-specific interactions was about  $19.2 \pm 2.2 \mu\text{g}/\text{cm}^2$ .

Moreover, SEM images of membrane surface before and after the c-(DMA-N<sub>3</sub>-BP-MAPS) coating and subsequent Bpt peptide conjugation highlighted that the polymer-peptide functionalization of PSf membranes does not modify the porosity of the native membrane (Fig. S4). Measurements with a capillary flow porometer revealed micropores with diameters of  $0.16 \pm 0.03$ ,  $0.15 \pm 0.01$ ,  $0.16 \pm 0.02$ , and  $0.16 \pm 0.01 \mu\text{m}$  for the native, c-(DMA-NAS-N<sub>3</sub>-MAPS)-Bpt, c-(DMA-NAS-N<sub>3</sub>-BP-MAPS)-Bpt, and c-(DMA-N<sub>3</sub>-BP-MAPS)-Bpt membranes, respectively (Table 3). Coherently the membrane porosity did not greatly vary with the functionalization process: values ranged from  $55 \pm 0.7\%$  for the

**Table 3**  
Structural properties of native and Bpt- functionalized membranes.

MEMBRANE	Mean flow pore size ( $\mu\text{m}$ )	Porosity (%)	Thickness ( $\mu\text{m}$ )	Ra (nm)	RMS (nm)
Native PSf	$0.16 \pm 0.03$	$55.0 \pm 0.7$	$129.7 \pm 1.0$	$25.5 \pm 0.5$	$33.8 \pm 1.1$
c-(DMA-NAS-N <sub>3</sub> -MAPS)-Bpt	$0.15 \pm 0.01$	$56.5 \pm 2.1$	$129.0 \pm 1.0$	$24.4 \pm 0.6$	$32.0 \pm 1.3$
c-(DMA-NAS-N <sub>3</sub> -BP-MAPS)-Bpt	$0.16 \pm 0.02$	$51.0 \pm 2.6$	$129.7 \pm 1.0$	$24.1 \pm 0.4$	$31.9 \pm 0.8$
c-(DMA-N <sub>3</sub> -BP-MAPS)-Bpt	$0.16 \pm 0.01$	$52.2 \pm 0.7$	$129.2 \pm 1.0$	$27.7 \pm 1.3$	$36.9 \pm 2.5$

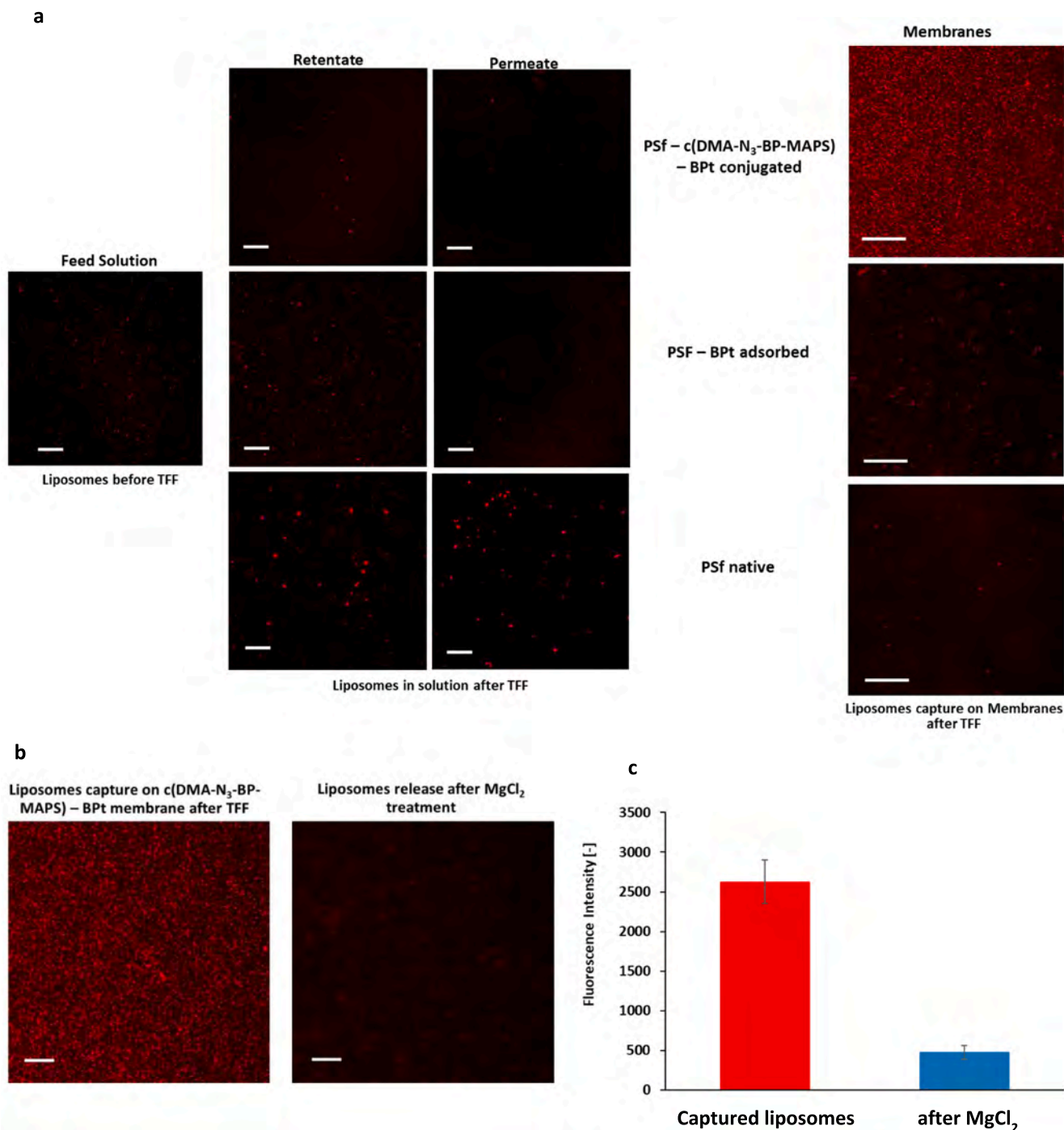


**Fig. 9.** CLSM images of liposome captured over c-(DMA-N<sub>3</sub>-BP-MAPS)-Bpt conjugated, Bpt adsorbed and native membranes and in the feed and the respective retentate/permeate solutions after TFF, scale bar 20 μm (a). Liposome capture over the c-(DMA-N<sub>3</sub>-BP-MAPS)-Bpt membranes and release after treatment with MgCl<sub>2</sub> scale bar 20 μm (b). Fluorescence intensity of captured liposomes and after MgCl<sub>2</sub> treatment (c).

native membrane to  $51 \pm 2.6\%$  for the c-(DMA-NAS-N<sub>3</sub>-BP-MAPS)-Bpt membrane. AFM analysis did not reveal significant changes of roughness parameters Ra and RMS between the native and functionalized membranes. The membranes have rather similar roughness values of Ra =  $25.5 \pm 0.5$  nm,  $24.4 \pm 0.6$  nm,  $24.1 \pm 0.4$  nm and  $27.7 \pm 1.3$  nm for the native, c-(DMA-NAS-N<sub>3</sub>-BP-MAPS)-Bpt, c-(DMA-NAS-N<sub>3</sub>-BP-MAPS)-Bpt, and c-(DMA-N<sub>3</sub>-BP-MAPS)-Bpt membranes, respectively. These findings clearly indicate that the peptide immobilization does not affect the membrane pore size and porosity, which are important features for the mass transfer and separation process. Moreover, the functionalization led to minor changes in the roughness of the membrane surfaces: the

roughness variation is less than 5 nm among the investigated membranes therefore this parameter cannot be considered dominant in this specific separation process.

#### 3.4. Liposome capture of functionalized membranes

The capacity of the peptide-functionalized membranes to capture nanovesicles was assessed in a model experiment by using liposomes in a tangential flow filtration system. Fluorescent liposomes of  $199 \pm 55$  nm size (Fig. S5), were tangentially flowed in the TFF cell unit over the c-(DMA-N<sub>3</sub>-BP-MAPS)-Bpt membrane. The capture efficiency was

compared with that obtained by TFF over native membranes and membranes where BPT was randomly adsorbed. The multifunctional c-(DMA-N<sub>3</sub>-BP-MAPS)-BPT membrane efficiently captured the flowed liposomes, as highlighted by the bright spots homogeneously distributed over the surface, visualized by CLSM after the TFF process (Fig. 9).

The membrane surface functionalization with BPT was able to recognize and bind liposomes. Differently, native membrane and membrane with randomly adsorbed peptide exhibited a low capacity to capture liposome particles: fluorescent liposomes flowed over and through the native membrane so that after the TFF process some of them were entrapped in the membrane wall, but most of them flowed in the retentate and permeate solutions (Fig. 9). Notably, liposome binding capacity observed in the case of c-(DMA-N<sub>3</sub>-BP-MAPS)-BPT membrane dramatically decreased when the peptide is non-specifically adsorbed onto the membrane surface likely due to unstable peptide-membrane interactions and poor exposure of peptide from the surface. As previously reported in microarray experiments, nanovesicles capturing efficiency is strictly bound to probes surface orientation [23]. The immobilization strategy by click chemistry allowed chemoselective binding and surface orientation of the immobilized peptides, which is crucial to maximize binding efficiency. After TFF, the liposomes bound to the membrane were released upon a mild treatment with divalent metal cations solution such as MgCl<sub>2</sub>. The results shown in Fig. 9b-c, indeed demonstrate the fully retained nanovesicles capturing ability of c-(DMA-N<sub>3</sub>-BP-MAPS)-BPT membrane and the subsequent release (about 82%) occurred after metal cations incubation, highlighted by the comparison of the fluorescence intensity for liposomes captured on the membrane and residual fluorescence after treatment with MgCl<sub>2</sub>. This indicates that BPT-liposome interaction can be conveniently reverted for isolation purposes.

We speculate that the metal cations thanks to their strong coordination ability can interfere with the established interactions between peptide and liposome on the membrane surface, allowing the release of liposomes in the eluting solution. The divalent cations can induce structural or conformational changes of the peptide chains interacting with the electron-donor groups (e.g., carboxylated groups) [36]. In particular, the carboxylate ion acts as a bidentate chelating ligand so as to coordinate the metal both by means of negatively charged oxygen and by carbonyl oxygen. Similar interactions can occur on the charged liposome surface, and the combined effect at the expense of the peptide-liposome interaction ultimately result in liposome release.

#### 4. Conclusions

In this paper we have successfully functionalized polysulfone membrane surface with nanometric copolymer coating and subsequent peptide conjugation to improve antifouling capacity and to enable nanovesicle capture. We have synthesized a family of copolymers with different functional groups and explored their use in the membrane modification to reduce non-specific interactions while promoting the conjugation of peptides able to bind highly curved lipid nanovesicles. Membranes coated with copoly azide polymers (c-(DMA-NAS-N<sub>3</sub>-MAPS), c-(DMA-NAS-N<sub>3</sub>-BP-MAPS), and c-(DMA-N<sub>3</sub>-BP-MAPS)) displayed a marked and stable wettability feature and deeply enhanced the Lewis-base sites over the membrane to values of ( $\gamma$ ) 43.15, 36.9 and 36.7 mJ/m<sup>2</sup>, respectively. It was demonstrated that the coating with the copoly azide polymers improves the filtration performance and antifouling capacity of membranes especially in the case of the membrane coated with c-(DMA-NAS-N<sub>3</sub>-BP-MAPS), and c-(DMA-N<sub>3</sub>-BP-MAPS) due to the coating ability to reduce protein adsorption of about 55–60%. Coated membranes were chemoselectively functionalized with the membrane sensing peptide BPT by click chemistry reaction with a density ranged from 26 to 28  $\mu\text{g}/\text{cm}^2$ . The capacity of the functionalized c-(DMA-N<sub>3</sub>-BP-MAPS)-BPT membrane to capture nanovesicles was assessed by using liposomes in a tangential flow filtration system. The capturing efficiency of the functionalized c-(DMA-N<sub>3</sub>-BP-MAPS)-BPT

membrane with respect to the membranes modified with adsorbed peptides and native membrane highlights the importance of the chemoselective binding and surface orientation to maximize the specific interaction between immobilized peptide and liposome. Furthermore, this functionalization strategy allows the peptide-nanovesicle interaction to be reverted, triggering the release and delivery of the vesicles (82%) after treatment with divalent metal cations.

#### CRedit authorship contribution statement

**Simona Salerno:** Writing – original draft, Methodology, Investigation. **Sabrina Morelli:** Investigation, Methodology. **Antonella Piscioneri:** Visualization, Investigation. **Mariangela Frangipane:** Investigation, Validation. **Alessandro Mussida:** Investigation, Methodology. **Laura Sola:** Visualization, Investigation. **Roberto Frigerio:** Visualization, Investigation. **Alessandro Strada:** Visualization, Investigation. **Greta Bergamaschi:** Visualization, Investigation. **Alessandro Gori:** Investigation, Methodology. **Marina Cretich:** Writing – review & editing. **Marcella Chiari:** Conceptualization, Writing – review & editing. **Loredana De Bartolo:** Conceptualization, Supervision.

#### Declaration of Competing Interest

The authors declare that they have no known competing financial interests or personal relationships that could have appeared to influence the work reported in this paper.

#### Acknowledgements

The Authors acknowledge the financial support from the European Union's Horizon 2020 research and innovation program under grant agreement No. 951768 (project MARVEL). The authors thank Dr. Maria Penelope De Santo, Department of Physics, University of Calabria, for the AFM measurements, and Dr. Roberto Consonni, Institute of Chemical Sciences and Technologies "G. Natta", National Research Council of Italy, for NMR analysis.

#### Appendix A. Supplementary material

Supplementary data to this article can be found online at <https://doi.org/10.1016/j.seppur.2022.121561>.

#### References

- [1] S. Morelli, A. Piscioneri, E. Curcio, S. Salerno, C.-C. Chen, L. De Bartolo, Membrane bioreactor for investigation of neurodegeneration, *Mater. Sci. Eng. C* 103 (2019) 109793, <https://doi.org/10.1016/j.msec.2019.109793>.
- [2] S. Salerno, E. Curcio, A. Bader, L. Diorno, E. Drioli, L. De Bartolo, Gas permeable membrane bioreactor for the co-culture of human skin derived mesenchymal stem cells with hepatocytes and endothelial cells, *J. Mem. Sci.* 563 (2018) 694–707, <https://doi.org/10.1016/j.memsci.2018.06.029>.
- [3] A. Piscioneri, H.M.M. Ahmed, S. Morelli, S. Khakpour, L. Diorno, E. Drioli, L. De Bartolo, Membrane bioreactor to guide hepatic differentiation of human mesenchymal stem cells, *J. Mem. Sci.* 564 (2018) 832–841, <https://doi.org/10.1016/j.memsci.2018.07.083>.
- [4] J. Aragón, S. Salerno, L. De Bartolo, S. Irusta, G. Mendoza, Polymeric electrospun scaffolds for bone morphogenetic protein 2 delivery in bone tissue engineering, *J. Colloid Interface Sci.* 531 (2018) 126–137, <https://doi.org/10.1016/j.jcis.2018.07.029>.
- [5] S. Salerno, A. Messina, F. Giordano, A. Bader, E. Drioli, L. De Bartolo, Dermal-epidermal membrane systems by using human keratinocytes and mesenchymal stem cells isolated from dermis, *Mater. Sci. Eng. C Mater. Biol. Appl.* 71 (2017) 943–953, <https://doi.org/10.1016/j.msec.2016.11.008>.
- [6] M. Colombo, G. Raposo, C. Théry, Biogenesis, secretion, and intercellular interactions of exosomes and other extracellular vesicles, *Annu. Rev. Cell Dev. Biol.* 30 (1) (2014) 255–289, <https://doi.org/10.1146/annurev-cellbio-101512-122326>.
- [7] K.M. Candelario, D.A. Steindler, The role of extracellular vesicles in the progression of neurodegenerative disease and cancer, *Trends Mol. Med.* 20 (7) (2014) 368–374, <https://doi.org/10.1016/j.molmed.2014.04.003>.
- [8] P. Vader, X.O. Breakefield, M.J.A. Wood, Extracellular vesicles: Emerging targets for cancer therapy, *Trends Mol. Med.* 20 (7) (2014) 385–393, <https://doi.org/10.1016/j.molmed.2014.03.002>.

- [9] D.A. Borrelli, K. Yankson, N. Shukla, G. Vilanilam, T. Ticer, J. Wolfram, Extracellular vesicle therapeutics for liver disease, *J. Control. Release* 273 (2018) 86–98, <https://doi.org/10.1016/j.jconrel.2018.01.022>.
- [10] A.J. O'Loughlin, C.A. Woffindale, M.J.A. Wood, Exosomes and the emerging field of exosome-based gene therapy, *Curr. Gene Ther.* 12 (2012) 262–274.
- [11] Z. Ye, T. Zhang, W. He, H. Jin, C. Liu, Z. Yang, J. Ren, Methotrexate-Loaded Extracellular Vesicles Functionalized with Therapeutic and Targeted Peptides for the Treatment of Glioblastoma Multiforme, *ACS Appl. Mater. Interfaces* 10 (15) (2018) 12341–12350, <https://doi.org/10.1021/acsami.7b18135>.
- [12] N. Yim, S.-W. Ryu, K. Choi, K.R. Lee, S. Lee, H. Choi, J. Kim, M.R. Shaker, W. Sun, J.-H. Park, D. Kim, W.D. Heo, C. Choi, Exosome engineering for efficient intracellular delivery of soluble proteins using optically reversible protein–protein interaction module, *Nat. Commun.* 7 (2016) 12277.
- [13] H.G. Lamparski, A. Metha-Damani, J.-Y. Yao, S. Patel, D.-H. Hsu, C. Ruegg, J.-B. Le Pecq, Production and characterization of clinical grade exosomes derived from dendritic cells, *J. Immunol. Methods* 270 (2) (2002) 211–226.
- [14] S. Kamerkar, V.S. LeBleu, H. Sugimoto, S. Yang, C.F. Ruivo, S.A. Melo, J.J. Lee, R. Kalluri, Exosomes facilitate therapeutic targeting of oncogenic KRAS in pancreatic cancer, *Nature* 546 (7659) (2017) 498–503, <https://doi.org/10.1038/nature22341>.
- [15] T. Baranyai, K. Herczeg, Z. Onódi, I. Voszka, K. Módos, N. Marton, G. Nagy, I. Mäger, M.J. Wood, S. El Andaloussi, Z. Pálkás, V. Kumar, P. Nagy, Á. Kittel, E. I. Buzás, P. Ferdinandy, Z. Giricz, M. Rito-Palomares, Isolation of exosomes from blood plasma: Qualitative and quantitative comparison of ultracentrifugation and size exclusion chromatography methods, *PLoS ONE* 10 (12) (2015) e0145686, <https://doi.org/10.1371/journal.pone.0145686>.
- [16] M.G. Moleirinho, R.J.S. Silva, M.J.T. Carrondo, P.M. Alves, C. Peixoto, Exosome-based therapeutics: Purification using semi-continuous multi-column chromatography, *Sep. Purif. Technol.* 224 (2019) 515–523, <https://doi.org/10.1016/j.seppur.2019.04.060>.
- [17] M.L. Heinemann, M. Ilmer, L.P. Silva, D.H. Hawke, A. Recio, M.A. Vorontsov, E. Alt, J. Vykoukal, Benchtop isolation and characterization of functional exosomes by sequential filtration, *J. Chromatogr. A* 1371 (2014) 125–135, <https://doi.org/10.1016/j.chroma.2014.10.026>.
- [18] S. Shin, D. Han, M.C. Park, J.Y. Mun, J. Choi, H. Chun, S. Kim, J.W. Hong, Separation of extracellular nanovesicles and apoptotic bodies from cancer cell culture broth using tunable microfluidic systems, *Sci. Rep.* 7 (2017) 9907, <https://doi.org/10.1038/s41598-017-08826-w>.
- [19] Y.-T. Yeh, Y. Zhou, D. Zou, H.e. Liu, H. Yu, H. Lu, V. Swaminathan, Y. Mao, M. Terrones, Rapid Size-Based Isolation of Extracellular Vesicles by Three-Dimensional Carbon Nanotube Arrays, *ACS Appl. Mater. Interfaces* 12 (11) (2020) 13134–13139.
- [20] K. Kim, J. Park, J.-H. Jung, R. Lee, J.-H. Park, J.M. Yuk, H. Hwang, J.H. Yeon, Cyclic tangential flow filtration system for isolation of extracellular vesicles, *APL Bioeng.* 5 (1) (2021) 016103, <https://doi.org/10.1063/5.0037768>.
- [21] L. Sola, F. Damin, P. Gagni, R. Consonni, M. Chiari, Synthesis of clickable coating polymers by postpolymerization modification: applications in microarray technology, *Langmuir* 32 (40) (2016) 10284–10295, <https://doi.org/10.1021/acs.langmuir.6b02816>.
- [22] L. Sola, D. Brambilla, A. Mussida, F. Consonni, F. Damin, M. Cretich, A. Gori, M. Chiari, A bi-functional polymeric coating for the co-immobilization of proteins and peptides on microarray substrates, *Anal. Chim. Acta* 1187 (2021) 339138, <https://doi.org/10.1016/j.aca.2021.339138>.
- [23] A. Gori, A. Romanato, B. Greta, A. Strada, P. Gagni, R. Frigerio, D. Brambilla, R. Vago, S. Galbiati, S. Picciolini, M. Bedoni, G.G. Daaboul, M. Chiari, M. Cretich, Membrane-binding peptides for extracellular vesicles on-chip analysis, *J. Extracell. Vesicles* 9 (2020) 1751428, <https://doi.org/10.1080/20013078.2020.1751428>.
- [24] B. Antonny, Mechanisms of membrane curvature sensing, *Annu Rev Biochem.* 80 (1) (2011) 101–123, <https://doi.org/10.1146/annurev-biochem-052809-155121>.
- [25] M. Mammen, G. Dahmann, G.M. Whitesides, Effective Inhibitors of Hemagglutination by Influenza virus synthesized from polymers having active ester groups. Insight into mechanism of inhibition, *J. Med. Chem.* 38 (21) (1995) 4179–4190.
- [26] F. Landi, C.M. Johansson, D.J. Campopiano, A.N. Hulme, Synthesis and Application of a New Cleavable Linker For “click”-Based Affinity Chromatography, *Org. Biomol. Chem.* 8 (1) (2010) 56–59.
- [27] L. Sola, F. Damin, M. Cretich, M. Chiari, Novel polymeric coatings with tailored hydrophobicity to control spot size and morphology in DNA microarray, *Sensor Actuator B Chem.* 231 (2016) 412–422, <https://doi.org/10.1016/j.snb.2016.03.049>.
- [28] M. Lu, X. Zhao, H. Xing, Z. Xun, S. Zhu, L. Lang, T. Yang, C. Cai, D. Wang, P. Ding, Comparison of exosome-mimicking liposomes with conventional liposomes for intracellular delivery of siRNA, *Int. J. Pharm.* 550 (1-2) (2018) 100–113, <https://doi.org/10.1016/j.ijpharm.2018.08.040>.
- [29] S. Salerno, M.P. De Santo, E. Drioli, L. De Bartolo, Nano- and Micro-Porous Chitosan Membranes for Human Epidermal Stratification and Differentiation, *Membranes* 11 (2021) 394, <https://doi.org/10.3390/membranes11060394>.
- [30] R.J. Good, C.J. van Oss, The modern theory of contact angles and the hydrogen bond components of surface energies, in: M.E. Schrader, G.I. Loeb (Eds.), *Modern Approaches to Wettability*, Springer US, Boston, MA, 1992, pp. 1–27, [https://doi.org/10.1007/978-1-4899-1176-6\\_1](https://doi.org/10.1007/978-1-4899-1176-6_1).
- [31] L. De Bartolo, S. Morelli, A. Bader, E. Drioli, Evaluation of cell behaviour related to physico-chemical properties of polymeric membranes to be used in bioartificial organs, *Biomaterials* 23 (12) (2002) 2485–2497.
- [32] L. De Bartolo, A. Gugliuzza, S. Morelli, B. Cirillo, A. Gordano, E. Drioli, Novel PEEK-WC membranes with low plasma protein affinity related to surface free energy parameters, *J. Mater. Sci. Mater. Med.* 15 (8) (2004) 877–883, <https://doi.org/10.1023/B:JMSM.0000036275.60508.50>.
- [33] E. Curcio, L. De Bartolo, G. Barbieri, M. Rende, L. Giorno, S. Morelli, E. Drioli, Diffusive and convective transport through hollow fiber membranes for liver cell culture, *J. Biotechnol.* 117 (3) (2005) 309–321, <https://doi.org/10.1016/j.jbiotec.2005.02.004>.
- [34] W. Zhai, H. Yu, H. Chen, L. Li, D. Li, Y. Zhang, T. He, Stable fouling resistance of polyethylene (PE) separator membrane via oxygen plasma plus zwitterion grafting, *Sep. Purif. Technol.* 293 (2022), 121091.
- [35] L. De Bartolo, E. Curcio, E. Drioli, Membrane systems for bioartificial organs and regenerative medicine, *De Gruyter* (2017), <https://doi.org/10.1515/9783110268010-001>.
- [36] H. Liu, K. Håkansson, Divalent metal ion-peptide interactions probed by electron capture dissociation of trications, *J. Am. Soc. Mass Spectrom.* 17 (12) (2006) 1731–1741, <https://doi.org/10.1016/j.jasms.2006.07.027>.